

## Study of thermal properties of the medium produced in Au+Au collisions at $\sqrt{s_{\text{NN}}} = 7.7 \text{ GeV}$ using a thermal model\*

V. Bairathi †

*Instituto de Alta Investigación,  
Universidad de Tarapacá, Arica 1000000, Chile  
vipul.bairathi@gmail.com*

D. Blaschke 

*Institute of Theoretical Physics,  
University of Wrocław, Max Born Pl. 1. 50-204 Wrocław, Poland*

L. Bravina 

*University of Oslo, P.O. Box 1048,  
Blindern, N-0316 Oslo, Norway*

W. K. Brooks

*Departamento de Física,  
Universidad Técnica Federico Santa María,  
Valparaíso, Chile*

T. Chhabra

*Department of Physics,  
University of Delhi, New Delhi, Delhi 110021, India*

*Department of Bioengineering,  
Indian Institute of Science,  
CV Raman Rd., Bengaluru, Karnataka 560012, India*

S. Kabana 

*Instituto de Alta Investigación,  
Universidad de Tarapacá, Arica 1000000, Chile*

S. Kuleshov 

*Universidad Andrés Bello,  
Avenida Repùblica 237, Santiago, Chile*

*Millennium Institute for SubAtomic  
Physics at the High-energy Frontier (SAPHIR) of ANID, Chile*

\* Based on a presentation at the 10th International Conference on New Frontiers in Physics (ICNFP 2021).

† Corresponding author.

I. Potashnikova

Departamento de Física,  
Universidad Técnica Federico Santa María,  
Avenida España 1680, Valparaíso, Chile

V. Sagun 

Centre for Physics of the University of Coimbra,  
Department of Physics,  
University of Coimbra, Coimbra, 3004-516 Portugal

O. Vitiuk 

Institute of Theoretical Physics,  
University of Wrocław,  
Max Born Pl. 1. 50-204 Wrocław, Poland

E. Zabrodin 

University of Oslo, P. O. Box 1048,  
Blindern, N-0316 Oslo, Norway  
Skobeltsyn Institute of Nuclear Physics,  
Moscow State University, 119991 Moscow, Russia

E. Zhrebtszoa 

Institute of Theoretical Physics,  
University of Wrocław,  
Max Born Pl. 1. 50-204 Wrocław, Poland

Received 29 October 2023

Revised 26 August 2024

Accepted 27 August 2024

Published 30 October 2024

In this study, we examine the thermal properties of the medium formed in ultra-relativistic heavy-ion collisions at chemical freeze-out using a thermal model. We utilize experimental data on various hadron species from 0% to 5% most central Au+Au collisions at  $\sqrt{s_{\text{NN}}} = 7.7 \text{ GeV}$  from the STAR BES program to analyze the thermal properties, namely, chemical freeze-out temperature, baryon chemical potential, and strangeness chemical potential. We employ a  $\chi^2$  minimization technique to obtain these thermal properties. Furthermore, we also obtain thermal properties with strangeness conservation condition and at zero potentials  $\mu_B/T = \mu_S/T = 0$ . We compare particle ratios from the thermal model with the experimental data. The thermal model describes particle ratios within  $\pm 2.5$  standard deviations and  $\chi^2/\text{NDF}$  between 1–2. We also discuss the collision energy dependence of thermodynamic properties of the medium at freeze-out and compare results with the published STAR results and other thermal model calculations.

*Keywords:* Thermal properties; quark-gluon plasma; heavy-ion collisions.

PACS numbers: 25.75.Dw

## 1. Introduction

Quantum chromodynamics (QCD) serves as the fundamental theory of strong interactions. It predicts a new state of matter under extreme conditions of

temperature and density in which quarks and gluons (partons) are no longer confined within hadronic matter. This state of matter is called quark-gluon plasma (QGP),<sup>1–4</sup> which can be produced in experiments through the collision of nuclei at ultra-relativistic energies. Exploring the properties of QGP is a crucial objective of high-energy heavy-ion collision experiments.<sup>5–8</sup>

The equilibrium thermodynamic properties of QCD matter can be determined by temperature ( $T$ ) and the three chemical potentials  $\mu_Q$ ,  $\mu_B$  and  $\mu_S$ . The strongly interacting system formed in heavy-ion collisions can be described by a QCD phase diagram.<sup>9,10</sup> By varying  $T$  and  $\mu_B$ , different phases of nuclear matter can be explored. Figure 1 shows a schematic picture of the QCD phase diagram.<sup>11</sup> In this diagram, the normal nuclear matter state is at  $T = 0$  and  $\mu_B \approx 938$  MeV. At high  $T$  and  $\mu_B$ , the phase of deconfined quarks and gluons is expected to be present, while at low  $T$  and  $\mu_B$ , the quarks and gluons are confined within hadrons.

Theoretically, the phases of QCD can be explored through numerical simulations on a space-time lattice in a nonperturbative QCD regime, known as lattice QCD.<sup>12,13</sup> Lattice QCD calculations at finite temperature ( $T > 0$ ) and zero baryon density ( $\mu_B = 0$ ) suggest that the parton–hadron phase transition evolves through a rapid crossover.<sup>14</sup> At finite  $T$  and  $\mu_B$ , lattice QCD<sup>15</sup> and several QCD-based models<sup>16–19</sup> propose a first-order phase transition. The endpoint of the first-order phase

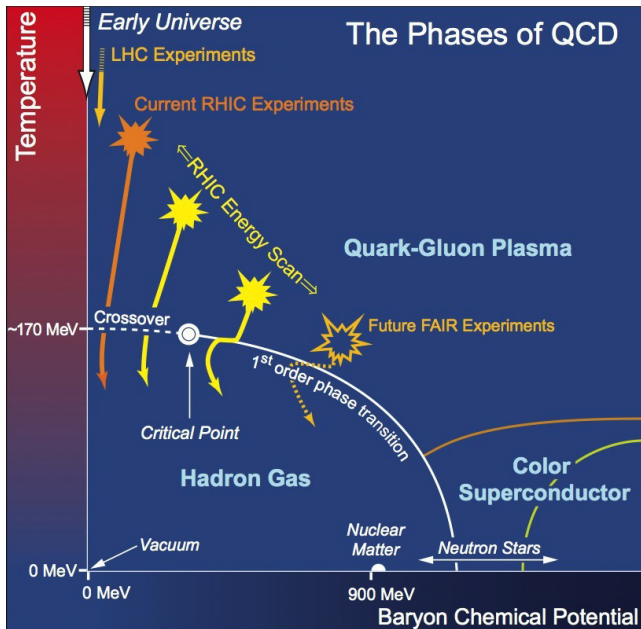


Fig. 1. Schematic diagram of the phases of QCD plotted as the temperature ( $T$ ) versus the baryon chemical potential ( $\mu_B$ ).<sup>9,11</sup> The solid lines show the conjectured boundaries for various QCD phases. The dotted curve marks the crossover transition between the hadronic and QGP matter. The solid circle depicts the possible location of a QCD critical point.<sup>20</sup>

transition in  $T$ - $\mu_B$  plane is the QCD critical point.<sup>21,22</sup> Experimentally, the phases of QCD can be explored by varying the center of mass energy of heavy-ion collisions. The temperature and baryon chemical potential depend on the collision energy ( $\sqrt{s_{\text{NN}}}$ ). The Relativistic Heavy-Ion Collider (RHIC) beam energy scan (BES) and heavy-ion program at the Large Hadron Collider (LHC) have provided a wide energy coverage to explore the QCD phase diagram.

In relativistic heavy-ion collisions, a highly dense fireball of quarks and gluons is created. The constituents of the fireball interact frequently, leading to the buildup of a radially outward pressure gradient during the thermalization process. This process leads to the space-time expansion and simultaneous cooling of the fireball. As the interactions among the constituents become weak, the space-time evolution ends, and the system undergoes chemical and kinetic freeze-out stages. The properties of the system at freeze-out can be studied through thermodynamic parameters such as temperature ( $T$ ) and chemical potentials ( $\mu$ ). Statistical and thermal models, described in Refs. 23–25, can be employed to determine these freeze-out parameters. These models utilize the  $\chi^2$  minimization procedure to fit the experimentally measured yields and ratios of various particle species. By studying the energy dependence of freeze-out properties, researchers can gain valuable insights into the transition from the deconfined QGP to ordinary hadronic matter, providing an important tool for exploring the QCD phase diagram.

In this proceedings, we present the thermal properties of the medium formed in heavy-ion collisions at chemical freeze-out. We use a statistical thermal model<sup>26</sup> to fit the experimentally measured ratios of various particle species. The yields of particles are taken from the published results in Au+Au collisions at  $\sqrt{s_{\text{NN}}} = 7.7 \text{ GeV}$  by the STAR experiment at RHIC.<sup>27</sup> In Sec. 2, we briefly describe the thermal model and procedure to extract thermal properties  $T$ ,  $\mu_B$  and  $\mu_S$ . In Sec. 3, we discuss calculations of statistical and systematic uncertainties on the extracted thermal parameters. In Sec. 4, we present the thermal parameters as a function of  $\sqrt{s_{\text{NN}}}$  and compare them with the published results from various other thermal models. At the end, in Sec. 5, we summarize the results.

## 2. Thermal Model

In this work, we utilize statistical and thermodynamic models to analyze the yields and ratios of identified particles generated in heavy-ion collisions. Our primary focus is to determine the phase boundary between the QGP and hadronic matter by examining thermal properties. We consider the thermodynamic potential of a grand canonical ensemble of hadron resonances without further interactions among them. We assume that the particles produced in collisions of nucleons or nuclei ( $p + p$ ,  $p + A$ ,  $A + A$ ) emerge from a thermal source. The thermodynamic variables are volume  $V$ , temperature  $T$ , baryon and strangeness fugacities  $\chi_B = \mu_B/T$  and  $\chi_S = \mu_S/T$ . The fugacity of the third component of isospin is set to zero, neglecting isospin asymmetries. Additionally, we investigate the equilibrium condition for both

phases to coexist when fugacities are vanishing. Our approach involves using the thermal model to determine the intensive thermodynamic parameters, which we then extrapolate to zero fugacities along states with equal entropy density, energy density, or density. The goal is to compare the temperature at zero fugacities with the initial energy density achieved in the collision to reveal a boundary reflecting the QCD phase transition. The detailed description of the thermal model can be found in Refs. 26 and 28.

## 2.1. Input parameters

The input parameters to the thermal model are fugacities  $\chi_B = \mu_B/T$  and  $\chi_S = \mu_S/T$ . The following equations are used to calculate the initial values of the two fugacities using the  $\bar{p}/p$  and  $K^-/K^+$  ratios.

$$e^{-2\mu_B/T} = \frac{\bar{p}}{p}, \quad e^{-2\mu_S/T} = \frac{K^-}{K^+}. \quad (1)$$

The initial values of input parameters calculated using Eq. (1) are  $\chi_B = 2.474$  and  $\chi_S = 0.4969$  for central Au+Au collisions at  $\sqrt{s_{NN}} = 7.7$  GeV. The input parameters are further optimized by varying their values in steps of 10% up to  $\pm 90\%$  of the initial values. A minimum  $\chi^2/\text{NDF}$  is obtained for each set of input parameters, and it is then plotted as a function of  $\mu_B/T$  and  $\mu_S/T$  as shown in Fig. 2.  $\mu_B/T$  and  $\mu_S/T$  corresponding to the minimum  $\chi^2/\text{NDF}$  are chosen as the final input parameters to calculate the thermal properties further. The input parameters obtained after the optimization are  $\chi_B = 2.721$  and  $\chi_S = 0.4969$ .

## 2.2. Thermal parameters

The thermal parameters are obtained using fits to the experimental data with the model calculations. Particle ratios are used to extract the parameters, namely,  $T$ ,  $\mu_B$  and  $\mu_S$  at chemical freeze-out. The volume ( $V$ ) parameter is canceled out due to the

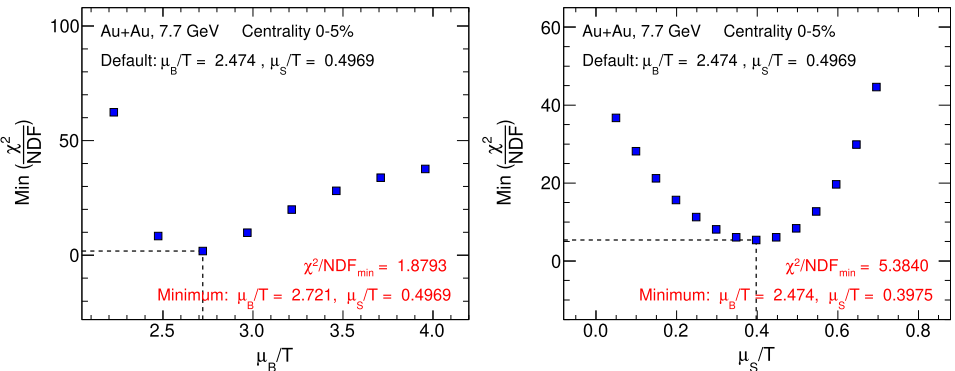


Fig. 2. The variation of  $\mu_B/T$  and  $\mu_S/T$  for central Au+Au collisions at  $\sqrt{s_{NN}} = 7.7$  GeV. The dashed line represents optimized values of the input parameters at the minimum  $\chi^2/\text{NDF}$ .

use of particle ratios. Also, ratios typically have a smaller systematic error than absolute yields. Therefore, we focus on ratios of particle yields in this work. The optimized input parameters  $\mu_B/T$  and  $\mu_S/T$  are used as the initial values to the model as discussed in Subsec. 2.1. A  $\chi^2$  minimization procedure is used to obtain the best fit. The  $\chi^2$  is defined as

$$\chi^2 = \sum_i \left( \frac{R_i^{\text{Th}} - R_i^{\text{exp}}}{\sigma_i^{\text{exp}}} \right)^2, \quad (2)$$

where  $R_i^{\text{exp}}$  is the experimentally measured value of the particle ratio with the corresponding uncertainty  $\sigma_i^{\text{exp}}$  and  $R_i^{\text{Th}}$  is the particle ratio value from the thermal model. The sum runs over the number of particle ratios available experimentally. The yields of particles are taken from results published by the STAR experiment at RHIC for most central (0–5%) Au+Au collisions to calculate the particle ratios used in this model.<sup>27</sup> Statistical and systematic uncertainties of the measured yields are added quadratically. The uncertainties on the particle ratios are obtained by propagating uncertainties of the particle yields. After that,  $\chi^2/\text{NDF}$  is plotted as a function of  $T$ ,  $\mu_B$  and  $\mu_S$  as shown in Fig. 3. The values of the thermal parameters are taken at the minimum of  $\chi^2/\text{NDF}$ .

An important aspect of the model is the contribution of feed-down from weak decays. The measurements from the experiment are generally corrected for the feed-down contributions. In this model, we subtract the feed-down contribution from weak decays following the relevant experimental papers. In particular,  $\pi$  and  $\Lambda$  yields are corrected for the weak decays while  $p$ ,  $K$  and  $\Xi$  are inclusive as in the data.

### 2.3. Particle ratios

The expected particle ratios from the thermal model are calculated at the chemical freeze-out. We compare experimental data to these predictions to assess the degree of agreement with the experimental data. Figure 4 shows a comparison between the experimental data (red circles) and thermal model predictions (solid blue lines). The difference between the experimental ratios and that predicted by the thermal model denoted by the standard deviation (SD) =  $(R^{\text{Th}} - R^{\text{exp}})/\sigma^{\text{exp}}$  are also shown in the

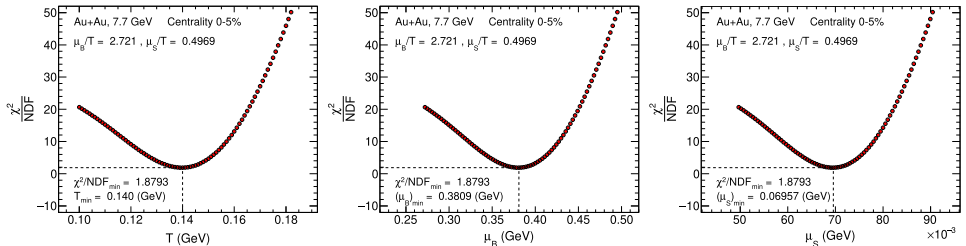


Fig. 3.  $\chi^2/\text{NDF}$  as a function of  $T$ ,  $\mu_B$  and  $\mu_S$  for central Au+Au collisions at  $\sqrt{s_{\text{NN}}} = 7.7$  GeV. The dashed lines represent the thermal parameters at the minimum  $\chi^2/\text{NDF}$ .

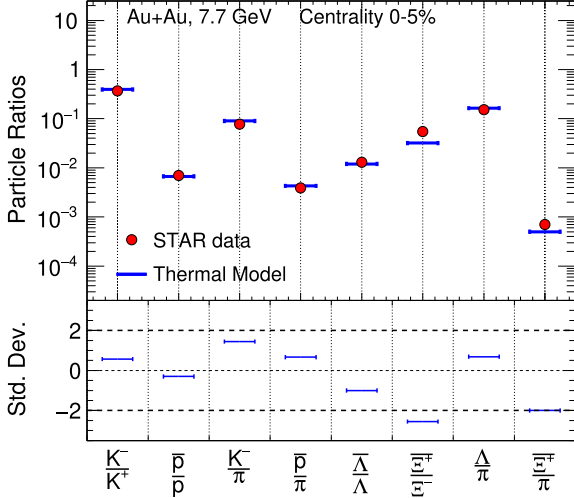


Fig. 4. (Color online) (Top panel) Particle ratios for most central (0–5%) Au+Au collisions at  $\sqrt{s_{\text{NN}}} = 7.7 \text{ GeV}$ . Red circles show ratios calculated from the experimental yields, and solid blue lines show thermal model predictions. The uncertainties on the experimental particle ratios are smaller than the symbol size. (Bottom panel) SD between the experimental and theoretical particle ratios.

bottom panel of Fig. 4. The deviation is within  $\pm 2.5$  for all the particle ratios for most central (0–5%) Au+Au collisions at  $\sqrt{s_{\text{NN}}} = 7.7 \text{ GeV}$ .

### 3. Statistical and Systematic Uncertainties

In this section, we discuss the calculation of statistical and systematic uncertainties on the extracted thermal parameters from the thermal model. The procedure to calculate statistical uncertainties on the thermal parameters is as follows. We first consider two cases for the input experimental ratios: (1) adding experimental errors to the experimental ratios  $R_i^{\text{exp}} = R_i^{\text{exp}} + \sigma_i^{\text{exp}}$ , (2) subtracting experimental errors from the experimental ratios  $R_i^{\text{exp}} = R_i^{\text{exp}} - \sigma_i^{\text{exp}}$ . We perform the fitting and  $\chi^2$  minimization as mentioned in Sec. 2 for the two cases and extracted  $T$ ,  $\mu_B$  and  $\mu_S$ . The maximum deviations of the two cases from the default case are taken as the statistical uncertainties on the extracted parameters.

The procedure for the systematic uncertainties on the thermal parameters is as follows. For this, we again consider two cases: (1) 100% correction of the weak decay to the calculated particle ratios from the thermal model and (2) without weak decay corrections. We then perform the fitting and  $\chi^2$  minimization mentioned in Sec. 2 for the two cases and extracted  $T$ ,  $\mu_B$  and  $\mu_S$ . The systematic uncertainties on the extracted parameters are taken to be the average of deviations of the two cases with respect to the default case.

The statistical and systematic uncertainties are added in quadrature to get total uncertainty on the thermal parameters. We also consider a strangeness conservation

case in which thermal parameters from the model are calculated with the condition  $s - \bar{s} = 0$  (i.e. the difference between strange and anti-strange quarks is zero). We include uncertainty due to the strangeness conservation and add it in quadrature to the total uncertainty.

## 4. Results

In this section, we present the results obtained from the thermal model in most central (0–5%) Au+Au collisions at  $\sqrt{s_{\text{NN}}} = 7.7$  GeV. We discuss collision energy dependence of the thermal parameters  $T, \mu_B$ . Comparison with the published results from other thermal model calculations is also discussed.

### 4.1. Energy dependence of the thermal parameters

Figure 5 shows collision energy dependence of thermal parameters from the thermal model for 0–5% central Au+Au collisions. The results are compared with published results from the STAR experiment as shown in blue stars.<sup>27</sup> We also compared the results from different thermal models taken from the references of Andronic *et al.*<sup>25</sup> and Cleymans *et al.*<sup>29</sup> The freeze-out temperature sharply increases with the collision energy below 10 GeV and then saturates at higher energies. The baryon chemical potential smoothly decreases as the collision energy increases. The freeze-out temperature and the baryon chemical potential from our model agree well with other thermal models and the STAR results and follow the same energy dependence.

### 4.2. Strangeness conservation

Figure 6 shows the collision energy dependence of the thermal parameters obtained with the strangeness conservation condition  $s - \bar{s} = 0$ . The results are shown in red

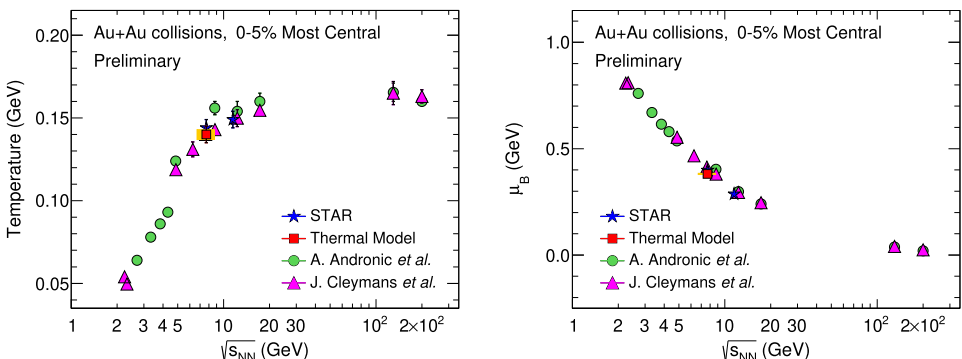


Fig. 5. (Color online)  $T$  (left panel),  $\mu_B$  (right panel) as a function of  $\sqrt{s_{\text{NN}}}$  from the thermal model for most central (0–5%) Au+Au collisions (red squares). The yellow band represents systematic uncertainties in the thermal parameters. Results from the STAR experiment are shown by blue stars.<sup>27</sup> Results from the thermal models of Andronic *et al.*<sup>25</sup> and Cleymans *et al.*<sup>29</sup> are shown by green circles and magenta triangles, respectively.

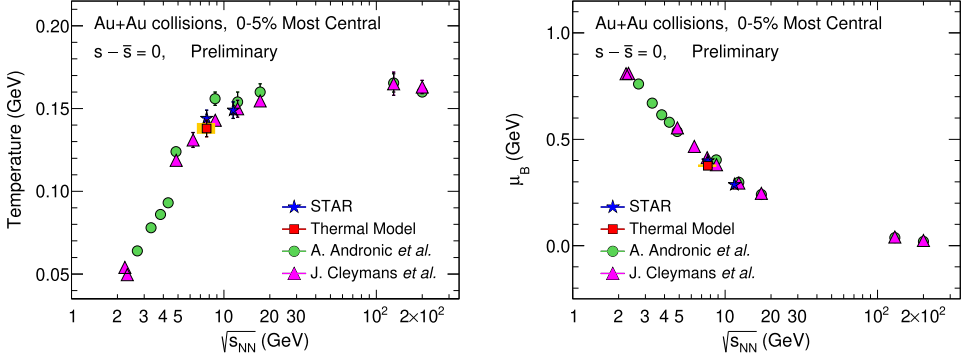


Fig. 6. (Color online)  $T$  (left panel),  $\mu_B$  (right panel) as a function of  $\sqrt{s_{NN}}$  from the thermal model for most central (0–5%) Au+Au collisions (red squares) with strangeness conservation. Blue stars show results from the STAR experiment. Results from the thermal models of Andronic *et al.*<sup>25</sup> and Cleymans *et al.*<sup>29</sup> are shown by green circles and magenta triangles, respectively.

squares for 0–5% central Au+Au collisions. The results are compared with other thermal model calculations from Andronic *et al.*<sup>25</sup> and Cleymans *et al.*<sup>29</sup> These results follow a similar energy dependence as without strangeness conservation. The temperature increases with collision energy and saturates for energies higher than 10 GeV, while the baryon chemical potential decreases with increasing collision energy. The freeze-out temperature and the baryon chemical potential from our model agree well with other models. Our model results also agree with that of the STAR experiment.

#### 4.3. Zero fugacities

Figure 7 shows the freeze-out temperature extrapolated to zero fugacities ( $\mu_B/T = \mu_S/T = 0$ ), keeping entropy density, energy density, or number density

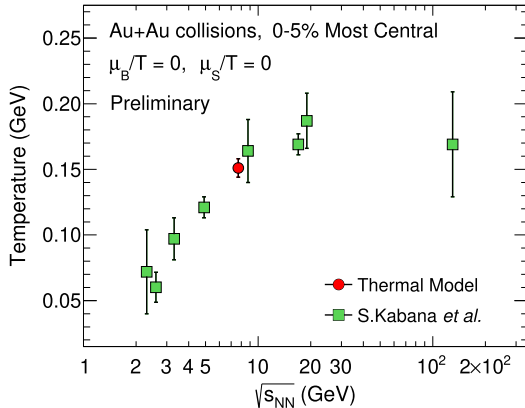


Fig. 7. (Color online) Temperature  $T$  as a function of  $\sqrt{s_{NN}}$  from the thermal model for most central (0–5%) Au+Au collisions (red circles) at zero fugacities ( $\chi_B = 0, \chi_S = 0$ ). Previously published results from the thermal models by Kabana *et al.* are shown in green squares.<sup>26,28</sup>

equal to the nonzero fugacities case. The results for the most central (0–5%) Au+Au collisions and previously published results by Kabana *et al.* are presented. The results from this work are consistent with results obtained for different data sets using the same thermal model and following the same energy dependence. This collision energy dependence of the temperature at zero fugacities with the initial energy density could be used to reveal a possible boundary, reflecting the QCD phase transition in relativistic heavy-ion collisions.

## 5. Summary

In this work, we obtain thermal properties such as  $T$ ,  $\mu_B$  and  $\mu_S$  for 0–5% most central Au+Au collisions at beam energy  $\sqrt{s_{NN}} = 7.7$  GeV using a thermal model. These results are obtained for the first time with our model, which presents several differences from other thermal models. We use an optimized set of initial parameters  $\mu_B/T$  and  $\mu_S/T$  to perform the thermal model analysis. We utilize various particle ratios to extract the thermal parameters. The experimental particle ratios are calculated from the particle yield results published by the STAR experiment at RHIC. The thermal model successfully describes the value of different particle ratios within  $\pm 2.5$  SD and  $\chi^2/NDF$  between 1–2. We employ a  $\chi^2$  minimization procedure to obtain chemical freeze-out temperature, baryon, and strangeness chemical potentials with and without strangeness conservation conditions. The freeze-out temperature is observed to increase with the collision energy and saturates for energies  $> 10$  GeV, while the baryon chemical potential decreases with increasing collision energy. We also obtain freeze-out temperature at zero fugacities to estimate a possible QCD phase transition boundary. The results for the thermal parameters at nonzero fugacities and their energy dependence are consistent with the STAR results and other thermal model calculations within uncertainties.

## Acknowledgments

The work of D. Blaschke was supported by the Polish National Science Center under Grant No. 2019/33/B/ST9/03059. V. Sagun acknowledges partial support by the Section of Physics and Astronomy of the National Academy of Science of Ukraine under Grant No. 0118U003197. V. Sagun is also thankful for the support by the Fundação para a Ciência e a Tecnologia (FCT), Portugal, under the Project Nos. UIDB/04564/2020, UIDP/04564/2020, EXPL/FIS-AST/0735/2021. L. Bravina and E. Zabrodin acknowledge support by the Norwegian Research Council (NFR) under Grant No. 255253/F50, “CERN Heavy Ion Theory”, and by the RFBR under Grants Nos. 1802-40084 and 18-02-40085. I. Potashnikova was supported in part by grants ANID- Chile FONDECYT 1170319, and W. Brooks BASAL ANID PIA/APOYOAFB180002. S. Kabana acknowledges partial support by ANID PIA/APOYO AFB220004 (Chile). S. Kuleshov, S. Kabana and W. Brooks acknowledge partial support by the Millennium Institute for SubAtomic Physics at the High-energy

FrontIer (SAPHIR), ICN2019\_044, ANID, Chile. S. Kuleshov acknowledges partial support by the grant FONDECYT 1191103, ANID, Chile.

## ORCID

- V. Bairathi  <https://orcid.org/0000-0003-3415-6911>  
D. Blaschke  <https://orcid.org/0000-0002-8399-5183>  
L. Bravina  <https://orcid.org/0000-0001-9679-5466>  
S. Kabana  <https://orcid.org/0000-0003-0568-5750>  
S. Kuleshov  <https://orcid.org/0000-0002-3065-326X>  
V. Sagun  <https://orcid.org/0000-0001-5854-1617>  
O. Vitiuk  <https://orcid.org/0000-0002-9744-3937>  
E. Zabrodin  <https://orcid.org/0000-0003-3093-6769>  
E. Zherebtsova  <https://orcid.org/0000-0002-1364-0969>

## References

1. T. D. Lee and G. C. Wick, *Phys. Rev. D* **9**, 2291 (1974).
2. J. C. Collins and M. J. Perry, *Phys. Rev. Lett.* **34**, 1353 (1975).
3. E. V. Shuryak, *Phys. Rep.* **61**, 71 (1980).
4. M. Gyulassy and L. McLerran, *Nucl. Phys. A* **750**, 30 (2005).
5. BRAHMS Collab. (I. Arsene *et al.*), *Nucl. Phys. A* **757**, 1 (2005).
6. PHENIX Collab. (K. Adcox *et al.*), *Nucl. Phys. A* **757**, 184 (2005).
7. PHOBOS Collab. (B. B. Back *et al.*), *Nucl. Phys. A* **757**, 28 (2005).
8. STAR Collab. (J. Adams *et al.*), *Nucl. Phys. A* **757**, 102 (2005).
9. B. Mohanty, *New J. Phys.* **13**, 065031 (2011).
10. P. B. Munzinger and J. Wambach, *Rev. Mod. Phys.* **81**, 1031–1050 (2009).
11. P. B. Munzinger and J. Stachel, *Nature* **448**, 302 (2007).
12. K. G. Wilson, *Phys. Rev. D* **10**, 2445 (1974).
13. M. Creutz, *Phys. Rev. D* **21**, 2308 (1980).
14. Y. Aoki *et al.*, *Nature* **443**, 675 (2006).
15. S. Ejiri, *Phys. Rev. D* **78**, 074507 (2008).
16. M. Asakawa and K. Yazaki, *Nucl. Phys. A* **504**, 668 (1989).
17. A. Barducci *et al.*, *Phys. Lett. B* **231**, 463 (1989).
18. A. Barducci *et al.*, *Phys. Rev. D* **41**, 1610 (1990).
19. M. A. Stephanov, *Prog. Theor. Phys. Suppl.* **153**, 139 (2004).
20. R. V. Gavai and S. Gupta, *Phys. Rev. D* **71**, 114014 (2005).
21. Z. Fodor and S. Katz, *J. High Energy Phys.* **04**, 50 (2004).
22. R. Gavai and S. Gupta, *Phys. Rev. D* **78**, 114503 (2008).
23. J. Cleymans and K. Redlich, *Phys. Rev. C* **60**, 054908 (1999).
24. F. Becattini, J. Manninen and M. Gazdzicki, *Phys. Rev. C* **73**, 044905 (2006).
25. A. Andronic, P. B. Munzinger and J. Stachel, *Nucl. Phys. A* **772**, 167 (2006).
26. S. Kabana and P. Minkowski, *New J. Phys.* **3**, 4 (2001).
27. STAR Collaboration (L. Adamczyk *et al.*), *Phys. Rev. C* **96**, 044904 (2017).
28. S. Kabana, *Eur. Phys. J. C* **21**, 545 (2001).
29. J. Cleymans *et al.*, *Phys. Rev. C* **73**, 034905 (2006).